Nanoscale

PAPER

View Article Online
View Journal

Cite this: DOI: 10.1039/c8nr03222j

Atomic scale reversible opto-structural switching of few atom luminescent silver clusters confined in LTA zeolites†

Saleh Aghakhani, [a] Didier Grandjean, *[a] Wouter Baekelant, [b] Eduardo Coutiño-Gonzalez, [b,c] Eduard Fron, [b] Kristina Kvashnina, [d,e] Maarten B. J. Roeffaers, [f] Johan Hofkens, [b] Bert F. Sels [f] and Peter Lievens [a]

Luminescent silver clusters (AgCLs) stabilized inside partially Ag exchanged Na LTA zeolites show a remarkable reversible on–off switching of their green-yellowish luminescence that is easily tuned by a hydration and dehydration cycle, making them very promising materials for sensing applications. We have used a unique combination of photoluminescence (PL), UV-visible-NIR Diffuse Reflectance (DRS), X-ray absorption fine structure (XAFS), Fourier Transform-Infrared (FTIR) and electron spin resonance (ESR) spectroscopies to unravel the atomic-scale structural changes responsible for the reversible optical behavior of the confined AgCLs in LTA zeolites. Water coordinated, diamagnetic, tetrahedral AgCLs $[Ag_4(H_2O)_4]^{2+}$ with Ag atoms positioned along the axis of the sodalite six-membered rings are at the origin of the broad and intense green-yellowish luminescence in the hydrated sample. Upon dehydration, luminescent $[Ag_4(H_2O)_4]^{2+}$ clusters are transformed into non-luminescent (dark), diamagnetic, octahedral AgCLs $[Ag_6(O_F)_{14}]^{2+}$ with Ag atoms interacting strongly with zeolite framework oxygen (O_F) of the sodalite four-membered rings. This highly responsive on–off switching reveals that besides quantum confinement and molecular-size, coordinated water and framework oxygen ligands strongly affect the organization of AgCLs valence electrons and play a crucial role in the opto-structural properties of AgCLs.

Received 19th April 2018,
Accepted 31st May 2018

DOI: 10.1039/c8nr03222j

rsc.li/nanoscale

Introduction

Few atom silver clusters (AgCLs) have received considerable attention in the last decade due to their unique electronic properties which strongly depend on their size and shape. Devising a protocol for tailoring their structure by stabilizing them inside proper host materials has significantly increased their potential in imaging, sensing, optoelectronic, catalytic and photocatalytic applications.[1–4] Zeolites as microporous aluminosilicate materials have been increasingly used as suitable scaffolds for encapsulation of small AgCLs (2–8 atoms) owing to their well-defined, quantum sized cages, channels and their facile ion exchange capability with metal precursor ions.[3–6] Zeolite topology, AgCLs charge, extra framework cations and hydration level are all tuneable parameters for tailoring and stabilizing molecular AgCLs in zeolites.[4–11]

Highly luminescent and photostable AgCLs confined within LTA and FAU zeolites feature large Stokes shifts and broad emission colours spanning over the whole visible range with promising applications in bio-imaging, sensing and photonics.[6,7,11] Their PL properties in terms of excitation and emission energy, and quantum yield (QY) depend remarkably on the zeolite topology, Ag loading, co-cations type (Li, Na, K, Ca) and hydration level.[4,6,7,12,13] For instance, emissive AgCLs in FAU zeolites with a nearly 100% QY were recently obtained by carefully tuning Na and Ag cations mobility and improving the structural order of the AgCLs.[6]

Structures of AgCLs in Na LTA zeolites among others have been extensively studied by Rietveld refinement X-ray diffraction (XRD),[14–18] electron spin resonance (ESR),[14,19–22] extended

[a]Department of Physics and Astronomy, Laboratory of Solid State Physics and Magnetism, KU Leuven, Celestijnenlaan 200D, 3001 Leuven, Belgium. E-mail: didier.grandjean@kuleuven.be
[b]Leuven Chem &Tech: Molecular Imaging and Photonics (MIP), KU Leuven, Celestijnenlaan 200F, 3001 Leuven, Belgium
[c]CONACYT – Centro de Investigación y Desarrollo Tecnológico en Electroquímica, Parque Industrial Querétaro, Sanfandila s/n, Pedro Escobedo 76703, Querétaro, Mexico
[d]Rossendorf Beamline at ESRF-The European Synchrotron, CS40220, 38043 Grenoble Cedex 9, France
[e]Helmholtz Zentrum Dresden-Rossendorf (HZDR), Institute of Resource Ecology, PO Box 510119, 01314 Dresden, Germany
[f]Leuven Chem &Tech: Centre for Surface Chemistry and Catalysis (COK), KU Leuven, Celestijnenlaan 200F, 3001 Leuven, Belgium

†Electronic supplementary information (ESI) available: Details of structural information including of EXAFS, FTIR and ESR spectroscopy. See DOI: 10.1039/c8nr03222j

X-ray absorption fine structure (EXAFS),[23–27] Fourier transform infrared (FTIR),[14,28,29] and transmission electron microscopy (TEM).[30,31] Linear Ag_3^+ and Ag_3^{2+},[16] tetrahedral Ag_4,[19] octahedral Ag_6^+ and Ag_6^{3+},[24] were suggested in low Ag loaded Na LTA, whereas Ag_5^{3+} (ref. 25) and octahedral Ag_6 surrounded with 8 Ag^+ (ref. 14, 15, 18 and 31) were proposed in its fully loaded counterpart. However, the detailed understanding of the dynamic interaction of AgCLs with the framework oxygen atoms (O_F) and/or extra-framework water ligands and its role in the cluster formation, structure and optical properties has not been achieved. This can be partly attributed to the structural sensitivity of the LTA zeolites and to the low stability of AgCLs, particularly when exposed to electrons,[30,31] X-ray[15–18,23–27] or γ-ray[19] irradiation, leading to incomplete and often contradictory results. Recently, DFT modelling of luminescent AgCLs in partially exchanged Na LTA zeolites has highlighted the major role played by extra-framework water ligands in the cluster absorption and emission properties.[10] Indeed, doubly charged tetrahedral water coordinated $[Ag_4(H_2O)_n]^{2+}$ clusters formed in the sodalite cages, were identified as the luminescent species with optical band gaps directly correlated with the number of AgCL water ligands.

Optical switching of confined AgCLs currently is a hot topic as it may enable applications involving luminescence sensing, molecular switches, or chemical logic gates.[32–34] Although it has recently been observed in MOF,[32] DNA[34,35] and thiol[36,37] templates, the underlying switching mechanism was not fully understood mainly due to the heterogeneous structure of the clusters.[38,39] The structural identification of both luminescent and non-luminescent (dark) confined AgCLs is crucial to understand how the functionalities of few atom clusters are controlled at the atomic level by a change of the AgCLs nuclearity or of the cluster ligands.[33]

In this paper, we report for the first time a reversible water tuneable optical and structural switch of luminescent AgCLs into their non-luminescent (dark) counterparts in partially Ag exchanged Ag_3Na_9LTA zeolite. We have applied a combination of XAFS, UV-Vis-NIR, PL, FTIR, and ESR spectroscopies to unravel the dynamical structural changes at the atomic scale responsible for switching the optical properties of AgCLs. Detailed understanding of the structural changes responsible for this optical switching may contribute to further improvement and rational design of AgCLs with promising new functionalities confined in zeolites and other scaffolds.

Experimental

Sample preparation

Confined AgCLs in Na LTA zeolites (parent zeolite, UOP) were obtained by exchanging Na LTA with Ag ions and calcination following a procedure fully described elsewhere.[7,11] The structural formula for Na LTA zeolites, after normalization of the total amount of T (T = Si or Al) atoms in the unit cell to 24, is $(Na^+)_{12}[Si_{12}Al_{12}O_{48}]$, where Na is the counter-balancing ion. The amount of Ag ions exchanged with Na_{12}LTA zeolites to prepare a low Ag loading Ag_3Na_9LTA sample is 3 out of 12 per normalized unit cell. The hydrated sample was dehydrated under vacuum (0.1 mbar pressure) up to 450 °C, cooled down to room temperature, and collected in an argon-filled glovebox, as the dehydrated sample. Finally, the rehydrated sample was obtained after exposing the dehydrated sample to ambient conditions.

Photoluminescence spectroscopy

Emission and excitation spectra were recorded using an Edinburgh Instruments FLS 980 spectrometer on samples placed in a quartz cuvette (1 mm path length) that was similarly described in our previous work.[6,12] The emission was collected in "front face mode" through the quartz cuvette and sent to a monochromator and photomultiplier tube (PMT) detector. From the separate emission spectra at varying excitation wavelengths, two-dimensional (2D) excitation–emission matrices were constructed; the raw data were corrected for background and noise, and plotted with a resolution of 1 nm × 1 nm. To compare the PL performance of the samples, the absolute QY was measured at maximum excitation using an integrating sphere (Labsphere, 100 mm diameter) coupled to the aforementioned spectrometer.[12]

UV-Visible-NIR DRS spectroscopy

A UV-Visible-NIR Lambda 950 PerkinElmer spectrometer equipped with a 150 mm diameter integrating sphere coated with Spectralon was used to record the DRS spectra from 200–2500 nm with 1 nm spectral resolution. Attenuators were used to remove the effect of background and noise. The samples placed in a quartz cuvette were sealed and mounted on a Teflon sample holder.

XAFS spectroscopy

XAFS data were collected at Ag K-edge (25 514 eV), in transmission mode at ROBL (BM20)[40] (final measurements) and DUBBLE (BM26A)[41] (test measurements) beamlines of The European Synchrotron Radiation Facility (ESRF, Grenoble, France). The ionization chambers were filled with Ar/He gas mixtures. Data were collected up to k = 13 Å^{-1} with typical acquisition times of 20 min (*i.e.*, 1–25 s per data point). Hydrated and rehydrated samples were measured as 13 mm diameter self-supporting pellets (pressed under 1.5 tons) under ambient conditions, whereas the dehydrated sample was analysed in a sealed glass capillary (0.01 mm thickness, 1 mm external diameter and 80 mm length) to protect it from rehydration. The moderate X-ray flux at BM20 and BM26A (*ca.* 10^{10}–10^{11} ph s^{-1}) allowed the measurement of the hydrated and rehydrated states of the sample without significant dehydration caused by the X-ray beam,[42] though some local dehydration was observed (see EXAFS analysis). In addition, each XAFS measurement scan was performed at different sample locations to avoid possible degradation induced by prolonged X-ray beam irradiation. Three to six spectra were averaged to improve the signal-to-noise ratio to an optimal level. Data reduction of the experimental X-ray absorption spectra was

carried out with the EXBROOK program while EXAFS refinements were performed with the EXCURVE package.[43] Phase shift and backscattering factors were calculated *ab initio* by using Hedin-Lundqvist potentials. EXAFS analysis was carried out with k^3 weighting as it gave the most useful information on AgCLs owing to its high sensitivity to heavy atoms.[6]

FTIR spectroscopy

FTIR spectra were collected in transmission mode in the mid IR range (500–4000 cm^{-1}) using a Nicolet 6700 FTIR spectrometer. In order to avoid IR peak saturation and enhance the resolution, the sample was diluted with KBr (Potassium bromide, IR grade) to make adequate thin wafers (15–20 mg, wafer thickness ~50 μm) suitable for transmission mode measurements. *In situ* measurements were made using a home-built transmission IR cell equipped with heating and cooling system, vacuum pump, purging gas connections, and two ZnSe windows transparent in the mid IR range. The cell was kept under vacuum conditions (0.1 mbar pressure). Background corrected FTIR spectra were recorded at 25 °C after the sample reached each specific temperature (see FTIR data) and cooled down with a similar thermal ramp (5 °C min^{-1}). Averaged spectra consisting of 128 measurements with a spectral resolution of 2 cm^{-1} were used to enhance the signal-to-noise ratio.

ESR spectroscopy

ESR spectra were recorded on a Bruker 200D-SRC device in X-ban with a sweep of 6800 T centred at 3450 T. The samples were loaded into high-quality quartz tubes that were inserted in the double rectangular TE_{104} cavity of the ESR spectrometer, which was cooled by liquid nitrogen to a temperature of 120 K.[6]

Thermogravimetric analysis

TGA was performed with a Q500 TGA device (TA instruments) to monitor the weight loss behaviour of the hydrated sample upon dehydration. The sample (10–15 mg) was loaded in a platinum sample holder and heated with a thermal ramp of 5 °C min^{-1} up to 550 °C under nitrogen gas flow (90 mL min^{-1}, 1 bar).

Results

Reversible optical switching

On–off PL switching of the hydrated sample upon dehydration and rehydration is illustrated in Fig. 1A–C that shows the 2D emission–excitation plots of as-prepared hydrated, dehydrated, and rehydrated Ag_3Na_9LTA samples, respectively. The presence of water and hydroxyl absorption bands in the hydrated and rehydrated sample is identified in the NIR range (1400–2250 nm), where the overtone of the hydroxyl (1450–1475 nm) and the combination of the water and hydroxyl (1900–1950 nm) vibrations[44] are clearly observed (more details are given in Fig. S1†). Hydrated and rehydrated states feature quasi identical emission–excitation behaviour, showing three excitation maxima at 310, 360 and 420 nm

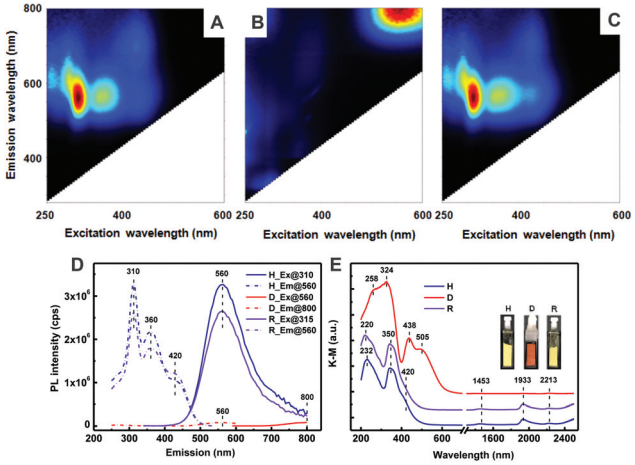

Fig. 1 2D excitation–emission plots of the sample in (A) the hydrated, (B) dehydrated, and (C) rehydrated state. (D) PL intensity of the sample at different excitation (Ex.) and emission (Em.) maxima in the hydrated (H), dehydrated (D) and rehydrated (R) state. (E) Diffuse reflectance UV-Visible-NIR spectra of the samples, the inset shows the actual colours of the sample in its different hydration states.

(Fig. 1D) with broad green-yellowish emission centred at 560 nm with 4.1 and 4.3% QY (@310 nm excitation) for the hydrated and the rehydrated states, respectively. The large emission spectral broadening could indicate the existence of a strong electron–phonon interaction between the confined AgCLs and zeolites structure.[45] Since the QY, water content and optical absorption (Fig. 1E) in both hydrated and rehydrated states of the sample are similar, the slight decrease in the excitation and emission intensity in the rehydrated compared to the hydrated state (Fig. 1D) is more likely originating from a different sample position and packing density in front phase mode PL measurement. The excitation spectrum corresponds to absorption transitions that are in line with previous reports that attributed mainly to luminescent AgCLs in low Ag loading LTA zeolite containing Na and K co-cations.[4,7,8,10] These excitation and emission bands were originally assigned to ligand to metal charge transfer (LMCT) upon the interaction of Ag cations with the O_F.[46–50] More recently, a DFT study attributed the green emission (with 350 nm excitation) observed in Ag LTA zeolites to doubly charged hydrated tetrahedral AgCLs, $[Ag_4(H_2O)_6]^{2+}$, where the contribution of Ag and water molecular orbitals were required for the occurrence of the luminescence.[10]

Upon full dehydration, as confirmed by the absence of the water and hydroxyl vibrational bands in the NIR range, the bright sample turned into a dark one (QY < resolution of the instrument @ 310 & 560 nm excitation). The 2D plot showed only a very faint emission at 800 nm that might be linked to larger AgCLs that are not likely to be highly emissive due to the existence of doublet or quartet ground states.

A reversible optical switching is also clearly demonstrated by UV-Visible-NIR DRS measurements, as presented in Fig. 1E. In the hydrated and rehydrated states, two intense UV absorp-

tion bands (220 and 350 nm) accompanied by a shoulder (420 nm) are observed. These bands are all attributed to the presence of Ag since the pure Na LTA showed no or little absorption within the UV-Visible range.[21,22,49] The high intensity of the 220 nm absorption was assigned to the $4d^{10}$ to $4d^{9}5s^{1}$ electronic transition of Ag cations that trigonally coordinate to the O_F.[20] The 350 nm absorption was attributed to the excitation of the luminescent AgCLs.[10,20,21] The broad shoulder at 420 nm responsible for the yellow colour of the sample (Fig. 1E, inset) was related to the LMCT from the O_F lone pairs to the low-lying 5s orbitals of Ag.[20,50,51] Besides, the 420 nm excitation produces an additional red band in the emission spectrum centred at 690 nm (Fig. 1A & C) that was assigned to the emission of a mixture of Ag_6^{2+} and Ag_6^{+} clusters that are abundant in fully Ag loaded LTA zeolites.[4] In contrast, DFT calculations attributed this band solely to $Ag_6(H_2O)_8^{4+}$ clusters.[10] Plasmon resonance absorption of Ag (within 400–600 nm) can be safely excluded here as no structural evidence of the presence of sufficiently large Ag^0 nanoparticles could be observed (see EXAFS analysis below). The small red shift of the absorption from 220 to 232 nm may be due to slight changes in the interaction level of Ag cations with the O_F and in their distribution in the LTA zeolites structure during the dehydration–rehydration cycle (see Table S1 and Fig. S5A†).

Upon dehydration of Ag_3Na_9LTA, a slight blue shift, a significant increase in the intensities of the UV-Vis absorption bands intensities from 256 to 324 nm, and the emergence of two additional visible bands (at 438 and 505 nm) are observed (Fig. 1E, inset). A similar increase in the absorption intensities was observed upon dehydration of Ag exchanged Na LTA zeolites.[20,52] This may be caused by the larger number of valence electrons found in larger Ag_6 clusters (see EXAFS results below), the more intense lower energy transitions associated with a smaller HOMO–LUMO gap, in line with the formation of larger AgCLs, and by the strong coordination of AgCLs to the zeolite O_F that generally forms several lower energy transitions in the UV-Vis range.[5,9] The two additional bands are responsible for the significant colour change from yellow to red-brick that also is associated to a change in the clusters nuclearity from Ag_4 to Ag_6 clusters.[20–22,52] Similar colour changes from white to yellow and dark brown were reported in other Ag containing compounds[18,53] and were mainly attributed to the decrease of the of Ag–O bond distance and the increase of their covalency (see Table S1†). Thus, the formation of larger AgCLs coordinated with O_F upon the loss of water ligands is likely explaining the significant increase in the absorption intensity and the remarkable sample colour change.

Reversible structural switching

To get a better understanding of the structural changes at the origin of the optical switching, a detailed Ag K-edge XAFS investigation of the hydrated and dehydrated Ag_3Na_9LTA was carried out. X-ray absorption near edge structure (XANES) is very useful for probing the oxidation state, coordination, and local symmetry of the absorbing atom while EXAFS is one of the most powerful techniques for investigating the structure of small clusters because it provides direct evidence of metal–metal, metal ligands bonds, and metal-support interaction.[54]

Although a precise correlation of the Ag edge position with the oxidation state is difficult to evaluate due to the considerable broadening of the spectrum related to short Ag core-hole life time,[55] Ag XANES data can be used complementary to monitor the structural evolution. Normalized XANES and their first derivatives (Fig. S2†) in the hydrated and rehydrated samples feature almost identical profiles. This indicates similar local environment of Ag atoms in both states. Slight differences between the XANES profiles of (re)hydrated and dehydrated samples are observed: a red shift of about 1.0 eV in the absorption edge and the formation of a small pre-edge structure in the dehydrated sample. The former is attributed to the reduction of Ag while the latter relates to the de-occupation of 4d orbitals of Ag possibly as a result of the formation of more covalent Ag–O bonds.[56,57] In addition, the edge position of Ag_3Na_9LTA samples lies between those of the Ag foil, Ag_2O, and $AgNO_3$ (Fig. S2B†) indicating the presence of intermediate valence states between Ag^0 and Ag^+ in line with previous reports that assigned them to the formation of partially charged AgCLs.[58]

The structural reversibility of AgCls in LTA zeolites is unravelled by the EXAFS analysis (Fig. 2). Sodalite cages in which AgCLs are stabilized, are composed of 8 single six rings (S6Rs) and 6 single four rings (S4Rs) which are connected through double four rings (D4Rs) forming a super cage (8 ring window). The detailed structure is presented in Fig. S3† including the different location sites of the extra-framework cations. To support the EXAFS analysis and build the precise 3D structures of AgCLs, the crystallographic data of a unit cell of a fully exchanged Ag_{12}LTA zeolite[17] were employed as they provided better agreement with our results than that of the Ag_3Na_9LTA structure. This is likely the consequence of the lack of long distance ordered structure in the LTA zeolite imposed by the high local concentration of Ag atoms in a small fraction of the sodalite cages (see below).

$\chi(k)$ k^3 weighted-EXAFS and the corresponding phase-corrected Fourier Transform (FT) best fits of the samples are presented in Fig. 2. EXAFS and FTs of hydrated and rehydrated

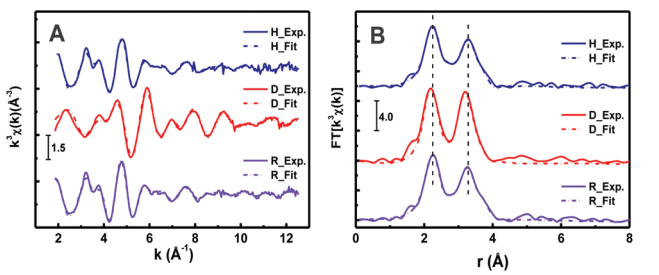

Fig. 2 (A) Ag K-edge k^3-weighted EXAFS and (B) corresponding phase corrected Fourier Transforms (FTs) best fits of the sample in the hydrated (H), dehydrated (D), and rehydrated (R) state. The experimental (Exp.) and fitted (Fit) data are indicated with solid and broken lines respectively, to visualize the fitting quality.

Ag_3Na_9LTA show similar profiles that differ significantly from those of the dehydrated sample. This suggests very similar structural environments around Ag atoms in both hydrated states, whereas in the dehydrated material a very different AgCLs structure is found. Among several possible EXAFS models that have been implemented to study AgCLs in LTA zeolites, a structural model based on Ag–O, Ag–Ag, and Ag–Si/Al shells[7,23] was applied as it gave the best agreement. In this model, a virtual mixed Si/Al site corresponding to a 50% Si : 50% Al occupancy is considered to reflect the Si to Al ratio of the LTA zeolites. Two main pronounced peaks in the range of 1.5–4.0 Å are observed in the FT profiles. The first intense peak can mainly be attributed to an Ag–O contribution (Ag–O: 2.2–2.8 Å), while the second multipeak consists of an Ag–Si/Al (3.25–3.32 Å) and two Ag–Ag contributions from AgCLs (Ag–Ag: 2.72–2.75 Å) and long range Ag–Ag distances between Ag atoms in the cluster (Ag_C) and Ag cations in the S6Rs, Ag_{6R} (3.31–3.47 Å). Details of the EXAFS analysis and the fitting parameters (Table S1) are given in the ESI.†

Based on the EXAFS analysis, 3D structures of AgCLs and their local environment inside the crystallographic structure of a sodalite cage of the LTA zeolite[17] were constructed and are presented in Fig. 3. For clarity purposes these structures are displayed in five separate views corresponding to columns I to V. Column I presents the complete atomic structure of AgCLs confined in the sodalite including the extra-framework ligands and Ag_{6R} and Na cations located in the S6Rs of the cage. In column II the sodalite has been removed and only the clusters coordinated to extra-framework water ligands are displayed. Column III is specifically depicting the interaction of Ag_C from AgCLs with zeolite O_F of S6Rs or S4Rs (O_{6R}/O_{4R}), while the actual positions of the single Ag or Na cations along the axis of the S6Rs are shown in Columns IV and V, respectively.

As anticipated by the XANES analysis, EXAFS fitting shows that the Ag based structure of the hydrated and rehydrated sample are virtually identical. In both states (Fig. 3A) a fraction of 66% of Ag atoms are coordinated to 3.0 Ag_c (CN_2/0.66, Table S1†) at 2.71–2.72 Å positioned on the axis of S6Rs inside the sodalite and forming tetrahedral-like Ag_4 clusters (column II), while the remaining part of the Ag cations (34%, Ag_{6R}) is located in the S6Rs of the sodalite surrounding the cluster (column V). Each Ag_c is either coordinated to ~2.4 O atoms of water molecules (O_w, 1.6/0.66, column II) at a distance of 2.36 Å or interacts directly with ~0.6 O_{6R} (CN_3/0.66, column III) at 3.17–3.18 Å, probably as a result of a local dehydration induced by the X-ray beam exposure[7] (see details in the ESI†). In these states, the sodalite contains a mixture of *ca.* 80% $[2.4\ O_w/(2.4\ O_w + 0.6\ O_{6R})]\ [Ag_4(H_2O)_4]$ and 20% (1–0.8) $[Ag_4(O_{6R})_2]$ clusters. Each Ag_c is surrounded by about 0.8 Na (CN_4/0.66, column III) and 0.4 Ag cations (Ag_{6R}, CN_6, column IV), which are both positioned on the axis of the S6Rs.

Upon dehydration (Fig. 3B), each Ag_c is now positioned along the axis of S4Rs inside the sodalite and is coordinated to 4.0 Ag_c (CN_2/0.38, Table S1†) forming octahedral Ag_6 clusters (column II). In the absence of water ligands, Ag_c interact directly with ~2.4 O_{4R} (CN_3/0.38) at 2.81 Å to form $[Ag_6(O_{4R})_{14}]$ clusters. Each Ag_c is surrounded further by ~1.3 Na (CN_4/0.38, column IV) and 0.6 Ag_{6R} (CN_6, column V) located in the S6Rs of the sodalite.

The degree of interaction between Ag_{6R}, Na cations and AgCLs and the zeolite framework is further detailed by *in situ* FTIR that is highly sensitive to the forces applied on the zeolite T–O–T (T = Si or Al) bond vibrations appearing between 1400 and 500 cm^{-1}. Coordination of metal clusters and cations with zeolites O_F leads to a weakening of the T–O framework bonds, and thus an elongation of the T–O distances accompanied by a change of the T–O–T angles[59–61] that are perturbing the asymmetric T–O–T stretching vibrations. This perturbation generates new bands within the 1200–900 cm^{-1} region[60–62] of the spectrum (Fig. S4 and S5†) along with the T–O–T vibrational band shifts proportional to the level of the cation–O_F interaction.[60] Upon dehydration of the sample, new T–O–T bands appear above 200 °C and become more pronounced once the temperature reaches 450 °C (Fig. S4A†) when dark Ag_6 clusters are formed (Fig. 3B). Furthermore, these bands undergo a red shift confirming that dehydration induces stronger interaction and a higher coordination of Ag and Na cations with the O_F atoms.

Upon re-coordination with water ligands dark Ag_6 clusters are integrally transformed back into the original luminescent mixture of Ag_4 clusters (Fig. 3A). Only a minor loss of reversibility is observed on the distribution of Na and Ag cations in S6Rs surrounding the Ag_4 clusters, as reflected by the total coordination number of Ag_{6R} surrounding Ag_C (CN_6) increasing from 0.4 to 1.2 after the dehydration–rehydration cycle. This indicates that a fraction of Na atoms in S6Rs surrounding the clusters has now been replaced by Ag atoms. This is likely a consequence of the general phenomenon of Ag aggregation in LTA zeolites favoured by the large cation mobility in these materials, ultimately at the origin of Ag cluster formation.[63] Indeed, the total number of Ag atoms (Ag_c + Ag_{6R}) in each of

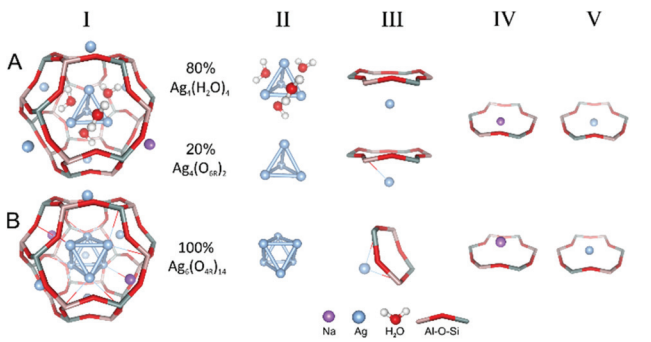

Fig. 3 Schematic 3D structure of AgCLs and their surrounding environments inside the sodalite cage of the sample in its (A) (re)hydrated and (B) dehydrated state. Complete atomic structure of the sodalite cage embedding the AgCLs including their extra-framework water ligands and the Ag and Na cations located in the S6Rs of the cage (I); AgCLs structural fraction depicting the presence or absence of the water ligands (II); interaction of the AgCLs atoms with the O_F of the sodalite S6Rs or S4Rs (III); actual positions of Na (IV) and Ag cations (V) along the axis of the S6Rs.

the sodalite cage containing AgCLs (Fig. 3) is much larger than the theoretical value of 3 derived from the Ag_3Na_9LTA stoichiometry. This confirms the strong local concentration of Ag in a limited fraction (*ca.* 25–50%) of the sodalites and thus validates the use of fully exchanged Ag_{12}LTA crystallographic data[17,18] to support our EXAFS models.

The precise charge identification of AgCLs was achieved indirectly with ESR spectroscopy in line with the XAFS results. ESR spectra of Ag_3Na_9LTA in both luminescent and dark states were silent (Fig. S6†) indicating that both Ag_4 and Ag_6 clusters are diamagnetic and feature an even positive charge. In the (re)hydrated states, Ag_4 clusters are doubly charged which is in agreement with a wide consensus on the formation and stabilization of diamagnetic AgCLs in low Ag loaded, hydrated Ag_xNa_{12-x}LTA or Ag_xK_{12-x}LTA zeolites ($x < 6$).[4,6,20] This is further supported by the XAFS results that showed the formation of partially charged Ag_4 clusters (Ag_4^{n+}) and by a recent DFT calculation[10] demonstrating the formation of luminescent Ag_4^{2+} clusters. In the dehydrated state, ESR suggests the formation of Ag_6^{n+} clusters with n = +2, +4 or +6. The formation of Ag_6^{2+} is supported by the XANES data (Fig. S2†) that shows a sharp decrease in the average charge per Ag_C forming the slightly reduced clusters upon dehydration (from +0.5 in Ag_4^{2+} to +0.33 in Ag_6^{2+}). ESR active lines of low Ag loaded Ag_xNa_{12-x}LTA zeolites reported earlier in several studies[20,24,63] were attributed to the presence of paramagnetic Ag_6^{+} clusters resulting from the coupling of the electron spin with six equivalent nuclear spins.[19–21,24,52,63] These ESR active AgCLs can only be observed upon H_2 activation or γ-irradiation[14,19,20,52,63] as demonstrated by the hyperfine splitting of ESR signal into seven lines observed after mild H_2 reduction of the dehydrated sample (Fig. S6†).

Discussion

Our EXAFS investigation allows unravelling the fine atomic tuning mechanism that is controlled by the hydration level of the LTA zeolite, and which is at the origin of the reversible optical switch of luminescent AgCLs. The green-yellowish luminescence observed in the hydrated and rehydrated states of the sample originates from tetrahedral Ag_4 clusters located in the centre of the sodalite cages, that are coordinated by 4 extra-framework water molecules. Similarly, in a DFT study of AgCLs in Na LTA zeolites, the green emission centred at 540 nm (350 nm excitation) displayed by the sample was assigned to a tetrahedral $[Ag_4(H_2O)_6]^{2+}$ cluster, coordinated to six water molecules.[10] The green luminescence is proposed to originate from a low-lying triplet excited state transition to the ground state molecular orbitals of Ag_4^{2+} cluster, that are mixed with oxygen of the water ligand. This complex luminescent configuration shows the importance of the water ligand field to obtain long-lived luminescent AgCLs in LTA zeolites.[10] Moreover, these results are in line with the luminescent properties of AgCLs that we recently identified with XEOL-detected EXAFS in Ag_3K_9LTA zeolites.[64] These cluster structures only differ by their average number of coordinated water molecules. A mixture of 60% $Ag_4(H_2O)_2^{2+}$ and 40% $Ag_4(H_2O)_4^{2+}$ species was found in Ag_3K_9LTA,[64] whereas in this report Ag_3Na_9LTA contains a mixture of 80% $Ag_4(H_2O)_4$ and 20% $Ag_4(O_{6R})_2$ clusters (Fig. 3A). $Ag_4(O_{6R})_2$ species were not detected in hydrated Ag_3K_9LTA zeolites suggesting that $Ag_4(H_2O)_x^{2+}$ clusters are more difficult to dehydrate when potassium is present as the counter-balancing cation. This may be due to the larger size of K^+ cations and to their lower mobility compared to that of Na^+.[63] It can also originate from the weaker interaction of K^+ relative to Na^+ cations with the water ligands due to their weaker Lewis acidic properties leading to better water ligands preservation of Ag_4^{2+} clusters during X-ray beam exposure.

The substantial transformation of the optical properties of the sample upon (vacuum) dehydration is directly linked to a large transformation of the cluster nuclearity and to alterations in the local environment of the clusters. The original Ag_4^{2+} clusters, coordinated to water molecules, are entirely converted into octahedral Ag_6^{2+} clusters upon the loss of water ligands and these larger clusters directly interact with the framework oxygen atoms (O_{4Rs}). The new clusters are non-luminescent, while their colour changes from pale yellow to brick-red. The appearance of two new bands centred at 438 and 505 nm in their absorption spectrum upon dehydration is responsible for the colour change (Fig. 1E, inset). This colour change was previously associated to the formation of Ag_6 clusters[15,17,22,65] or Ag cations coordinated with framework O_{4Rs} and strongly interacting with adjacent Ag cations coordinated with the O_{6Rs}.[50,51] Our investigation shows that the more intense and blue shifted main absorption band (from 350 to 324 nm, Fig. 1E) and the brick-red colour of dehydrated sample are all due to the formation of dark octahedral $Ag_6(O_{4R})_{14}^{2+}$ clusters inside the sodalites interacting both with O_{4R} and Ag_{6R} (Fig. 3B, column II, III, IV). Highly efficient coupling of AgCLs in their excited state to the electron trapping sites within Na LTA zeolite[66] and MLCT from AgCLs to the O_F upon their strong framework interaction could thus account for the non-luminescent properties of these clusters.

These results demonstrate that the LTA zeolite (steric) confinement itself is not sufficient to stabilize a particular type of cluster. AgCLs either coordinate to water ligands and form hydrated tetrahedral Ag_4^{2+} clusters or coordinate to the framework oxygen atoms (O_{4Rs}) and form framework-linked octahedral Ag_6^{2+} clusters. Yet, the structural and symmetrical constrains of the sodalite also affect the geometrical structure of AgCLs (Fig. 3 & Table S1†). Tetrahedral hydrated Ag_4^{2+} clusters are oriented along the axis of the S6Rs, where the Ag_C atoms of the clusters interact very weakly with the framework O_{6R} located at long distances [3.17 Å (R_3), 0.6 (CN_3/0.66)]. On the other hand, water-free octahedral Ag_6^{2+} clusters are oriented preferably along the S4Rs axis where Ag_C are strongly interacting with the framework O_{4R} [2.81 Å (R_3), 2.4 (CN_3/0.38)] located at shorter distances and therefore more prone to form dark AgCLs upon the loss of their water ligands.

Dynamic opto-structural reversibility, stimulated by the presence of water is facilitated by the weak Ag–Ag interaction

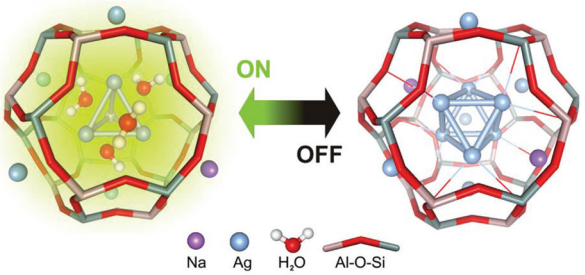

Fig. 4 Schematic representation of the reversible opto-structural switching of AgCLs confined in Ag_3Na_9LTA sodalites.

among AgCLs atoms (large Debye–Waller term, A_2 in Table S1†) and by the cation mobility in zeolites corresponding to electrical conductivity variations.[67,68] The full structural reversibility of the $Ag_4(H_2O)_4^{2+} \leftrightarrow Ag_6(O_{4R})_{14}^{2+}$ cluster transformation (Fig. 4) suggests that the two additional Ag atoms are most likely Ag_{6R} atoms of the same sodalite located at very short 3.42 Å distance (R_6) from Ag_C. Upon removal of water ligands from Ag_4^{2+}, two Ag_{6R} leave their position to merge with the Ag_4^{2+} cluster and move back to their original position upon rehydration of the Ag_6^{2+} cluster. This interpretation is in good agreement with previous electrical conductivity measurements of the Ag Na LTA system,[68] where the significant decrease of conductivity upon dehydration was attributed to the formation of larger AgCLs at the expense of Ag cations charge carrier consumption. In this scenario, the balance of zeolite framework charge upon the formation of larger Ag_6^{2+} clusters $[Ag_4(H_2O)_4^{2+} + 2Ag^+ \leftrightarrow Ag_6(O_{4R})_{14}^{2+} + 2X^+]$ could be compensated by H^+ exchange reactions with the zeolite framework as a result of water splitting.[69,70] However, the fact that OH was not detected neither in EXAFS nor in FTIR or NIR, may be due to the harsh dehydration conditions employed in this work or indicate the occurrence of water oxidation instead of water dissociation reaction.

This cluster transformation also highlights the important role of the co-cation type as Ag exchanged potassium LTA (Ag_3K_9LTA) did not show such clear reversible switching of the optical properties (Fig. S7†). We speculate that the lower diffusion rate (mobility) of K^+ cations relative to Na^+ and Ag^+ (cationic mobility of $K^+ < Ag^+ < Na^+$)[63] may explain the longer time required to establish the Ag_4–Ag_6 interconversion in Ag_3K_9LTA. In fact, two competitive forces are acting on Ag cations in Ag exchanged LTA zeolites: (i) stabilization of the negative charge of the zeolite framework by Ag cations covalently bonded to the O_{6R} of the S6Rs, and (ii) formation of AgCLs, whose relative equilibrium is displaced by the hydration level and co-cation type.

The results also show that different types of AgCLs are responsible for the luminescence and the colours of Ag exchanged Na LTA zeolites. This is in contradiction with previous studies claiming that single Ag^+ cations residing in the S6Rs of the sodalite are at the origin of the luminescence in these materials, as a result of LMCT from the O_F to Ag^+ single cations.[46,47,49,50,71] This controversy might be attributed to a confusion between the absorption at the origin of the luminescence and the sample colour, for which the excitation and absorption energy are different. For instance, the yellow colour of the hydrated sample (Fig. 1E) shows a lower absorption energy (420 nm) compared to the main absorption of Ag_4^{2+} (350 nm), which is more pronounced and red shifted in the dehydrated state (438 & 505 nm). This lower energy electronic transition assigned either to Ag_6 clusters[4,20] or to LMCT from the O_F to Ag cations[50,51] is distinct from the HOMO–LUMO gap of green luminescent Ag_4^{2+} that mainly consist of 5s–5p transition within AgCLs molecular orbitals.[10]

This study demonstrates the major role played by water molecules in precisely and reversibly controlling at the atomic scale the functional luminescent properties of AgCLs confined in zeolite templates. AgCLs size, nuclearity, configuration, charge and particularly its degree of coordination with the framework oxygen ($O_{4R/6R}$) are directly linked to the optical properties of AgCLs, besides the well documented size and confinement effect.[4,21,25,48,63] It also confirms that both quantum confinement and water coordination are indispensable structural requirements to create luminescent AgCLs in Ag LTA zeolite systems. These findings add valuable new information to the results of previous studies attributing luminescence of AgCLs solely to the existence of confined molecular Ag_3–Ag_6 clusters in the sodalite cages.[4,21,25,48,63]

This fully reversible and sharp "on/off" switch of AgCLs between two distinct optical states precisely tuned at the atomic level offers a new range of signal transduction mechanisms for molecular sensing that is likely to result in new designs with other scaffolds for multiple applications. Zeolite-stabilized AgCLs can be utilized as optical humidity sensor platforms, erasable optical memory, and molecular beacon probes for evaluation of guest–host interaction at atomic scale by measuring the interaction strength of the AgCLs with the zeolite O_F. Furthermore, the water induced reversible structural transformation of AgCLs in LTA zeolites can be introduced as a proof of principle for facile molecular tailoring of metal clusters in zeolites. It is reasonable to expect that this opto-structural switching can be repeated over several cycles as previous studies confirmed the strict reproducibility of the emission and absorption variation in Ag_xNa_{12-x}LTA zeolites upon up to ten consecutive hydration–dehydration treatments.[7,48]

This reversible $Ag_4^{2+} \leftrightarrow Ag_6^{2+}$ switching highlights the importance of the AgCLs charge and valence electrons in the modulation of their optical properties. Indeed, DFT modelling has shown that encapsulated few-atom AgCLs possessing a closed electronic shell (Ag_4^{2+}, Ag_6^{4+}) and behaving as "superatoms"[5,64,72] may be responsible for the strong absorption and luminescence observed in ZSM-5 zeolites,[5,9] LTA zeolites,[10] glass[73] and tryptophan.[74] Similar cluster nuclearities (Ag_4–Ag_6), geometries, short Ag–Ag bond distances (2.68 to 2.84 Å) and ligand coordination were obtained regardless of the template type. This suggests that similar cluster structure, electronic properties, and switching mechanisms may apply to AgCLs confined in various inorganic templates, but also in organic scaffolds such as DNA, MOF, thiol, protein, among

others. Interestingly, a similar reversible on–off transformation involving AgCLs has recently been observed in MOF[32] and DNA[34,35] although the mechanism of switching was not fully elaborated. The on–off reversible switching from red-emitting to dark species, clearly caused by an increase in the number of AgCLs turned on by the guanine bases ligand proximity,[75] reported in the DNA-templated AgCLs is now at the core of a new class of biosensors.[76]

These experimental and theoretical results suggest that luminescent AgCLs stabilized in various media and featuring similar optical behaviour may also share similar structural and electronic properties. As the structural identification of both luminescent and non-luminescent (dark) AgCLs confined in the rigid template of zeolites is facilitated by their high homogeneity, our results may contribute to the elucidation of the bright and dark structure of the AgCLs encapsulated in more heterogeneous scaffolds such as glass, DNA, thiols, *etc*.

Conclusions

Hydration–dehydration of partially Ag exchanged LTA zeolites (Ag_3Na_9LTA) induce a remarkable reversible optical switch that is closely associated with the atomic scale structural dynamics of AgCLs confined in the sodalite cages of LTA zeolites. In the (re)hydrated states, AgCLs show a broad green-yellowish emission attributed to the presence of hydrated, diamagnetic, tetrahedral Ag_4 clusters $[Ag_4(H_2O)_4]^{2+}$. Upon dehydration, hydrated Ag_4 clusters are transformed into dark, water-free, diamagnetic, octahedral Ag_6 clusters $[Ag_6(O_{4R})_{14}]^{2+}$, which strongly interacts with the oxygen atoms of the sodalite four rings (O_{4R}). Water and co-cation types play a crucial role in the opto-structural switch highlighting the high sensitivity of few atom clusters functional properties towards atomic scale structural changes. This reversible high-contrast opto-structural switching of AgCLs in LTA zeolites is a unique and responsive model system that has multiple potential applications as humidity sensor, erasable optical memory and guest–host interaction strength molecular probe. By unravelling the different structural features that control the optical properties of AgCLs, this work is paving the way for tuning the optical properties of AgCLs entrapped in LTA but also in other inorganic templates where they feature similar structures and PL. An in-depth investigation of the excited state dynamics expected to provide a broad understanding of the structure-to-function relationship and on the processes involved is currently underway.

Conflicts of interest

The authors declare no competing financial interest.

Acknowledgements

The authors gratefully acknowledge financial support from the Research Foundation Flanders (FWO) grants (G0990.11, G.0197.11, G.0962.13, G.0B39.15), the European Union's Seventh Framework Programme (FP7/2007-2013 under grant agreements no. 310651 SACS, no. 607417 CATSENSE and no. 307523 ERC-Stg LIGTH to M. B. J. R.), the Flemish government in the form of long-term structural funding "Methusalem" grant METH/15/04 CASAS2, the Hercules foundation (HER/11/14), the "Strategisch Initiatief Materialen" SoPPoM program. Access to DUBBLE was arranged through the support of FWO for use of the central facilities. The authors thank the staff of ROBL-BM20 and DUBBLE-BM26A (26-01-1027) beamlines of the ESRF for their assistance and technical support, and UOP Antwerp for the kind donation of zeolite material. The authors thank B. Dieu for the preparation of graphical material. E. Coutiño-Gonzalez gratefully acknowledges the support provided by Cátedras CONACYT.

Notes and references

1 J. T. Petty, S. P. Story, J. C. Hsiang and R. M. Dickson, *J. Phys. Chem. Lett.*, 2013, **4**, 1148–1155.
2 K. Shimizu, K. Sawabe and A. Satsuma, *Catal. Sci. Technol.*, 2011, **1**, 331–341.
3 I. Diez and R. H. A. Ras, *Nanoscale*, 2011, **3**, 1963–1970.
4 G. De Cremer, E. Coutino-Gonzalez, M. B. Roeffaers, B. Moens, J. Ollevier, M. Van der Auweraer, R. Schoonheydt, P. A. Jacobs, F. C. De Schryver, J. Hofkens, D. E. De Vos, B. F. Sels and T. Vosch, *J. Am. Chem. Soc.*, 2009, **131**, 3049–3056.
5 T. Yumura, M. Kumondai, Y. Kuroda, T. Wakasugi and H. Kobayashi, *RSC Adv.*, 2017, **7**, 4950–4959.
6 O. Fenwick, E. Coutino-Gonzalez, D. Grandjean, W. Baekelant, F. Richard, S. Bonacchi, D. De Vos, P. Lievens, M. Roeffaers, J. Hofkens and P. Samori, *Nat. Mater.*, 2016, **15**, 1017–1022.
7 E. Coutino-Gonzalez, W. Baekelant, D. Grandjean, M. B. J. Roeffaers, E. Fron, M. S. Aghakhani, N. Bovet, M. Van der Auweraer, P. Lievens, T. Vosch, B. Sels and J. Hofkens, *J. Mater. Chem. C*, 2015, **3**, 11857–11867.
8 N. T. Cuong, H. M. Nguyen and M. T. Nguyen, *Phys. Chem. Chem. Phys.*, 2013, **15**, 15404–15415.
9 T. Yumura, A. Oda, H. Torigoe, A. Itadani, Y. Kuroda, T. Wakasugi and H. Kobayashi, *J. Phys. Chem. C*, 2014, **118**, 23874–23887.
10 N. T. Cuong, H. M. Nguyen, M. P. Pham-Ho and M. T. Nguyen, *Phys. Chem. Chem. Phys.*, 2016, **18**, 18128–18136.
11 G. De Cremer, E. Coutino-Gonzalez, M. B. Roeffaers, D. E. De Vos, J. Hofkens, T. Vosch and B. F. Sels, *ChemPhysChem*, 2010, **11**, 1627–1631.
12 E. Coutino-Gonzalez, M. B. J. Roeffaers, B. Dieu, G. De Cremer, S. Leyre, P. Hanselaer, W. Fyen, B. Sels and J. Hofkens, *J. Phys. Chem. C*, 2013, **117**, 6998–7004.
13 G. De Cremer, Y. Antoku, M. B. Roeffaers, M. Sliwa, J. Van Noyen, S. Smout, J. Hofkens, D. E. De Vos, B. F. Sels and T. Vosch, *Angew. Chem., Int. Ed.*, 2008, **47**, 2813–2816.

14 T. Sun and K. Seff, *Chem. Soc. Rev.*, 1994, **94**, 857–870.
15 Y. Kim and K. Seff, *J. Phys. Chem.*, 1987, **91**, 671–674.
16 L. R. Gellens, W. J. Mortier and J. B. Uytterhoeven, *Zeolites*, 1981, **1**, 11–18.
17 L. R. Gellens, W. J. Mortier, R. A. Schoonheydt and J. B. Uytterhoeven, *J. Phys. Chem.*, 1981, **85**, 2783–2788.
18 Y. Kim and K. Seff, *J. Am. Chem. Soc.*, 1978, **100**, 6989–6997.
19 T. Wąsowicz and J. Michalik, *Int. J. Rad. Appl. Instrum., C*, 1991, **37**, 427–432.
20 R. A. Schoonheydt, *J. Phys. Chem. Solids*, 1989, **50**, 523–539.
21 J. Texter, R. Kellerman and T. Gonsiorowski, *J. Phys. Chem.*, 1986, **90**, 2118–2124.
22 R. A. Schoonheydt, *J. Mol. Catal.*, 1984, **27**, 111–122.
23 T. Yamamoto, S. Takenaka, T. Tanaka and T. Baba, *J. Phys.: Conf. Ser.*, 2009, **190**, 012171.
24 A. Baldansuren, H. Dilger, R. A. Eichel, J. A. van Bokhoven and E. Roduner, *J. Phys. Chem. C*, 2009, **113**, 19623–19632.
25 H. Hoshino, Y. Sannohe, Y. Suzuki, T. Azuhatai, T. Miyanaga, K. Yaginuma, M. Itoh, T. Shigeno, Y. Osawa and Y. Kimura, *J. Phys. Soc. Jpn.*, 2008, **77**, 064712.
26 Y. Suzuki, T. Miyanaga, H. Hoshino, N. Matsumoto and T. Ainai, *Phys. Scr.*, 2005, **115**, 765–768.
27 T. Miyanaga, H. Hoshino and H. Endo, *J. Synchrotron Radiat.*, 2001, **8**, 557–559.
28 M. D. Baker, G. A. Ozin and J. Godber, *J. Phys. Chem.*, 1985, **89**, 305–311.
29 M. D. Baker, J. Godber and G. A. Ozin, *J. Phys. Chem.*, 1985, **89**, 2299–2304.
30 A. Mayoral, T. Carey, P. A. Andersen and I. Diaz, *Microporous Mesoporous Mater.*, 2013, **166**, 117–122.
31 A. Mayoral, T. Carey, P. A. Anderson, A. Lubk and I. Diaz, *Angew. Chem., Int. Ed.*, 2011, **50**, 11230–11233.
32 R.-W. Huang, Y.-S. Wei, X.-Y. Dong, X.-H. Wu, C.-X. Du, S.-Q. Zang and T. C. W. Mak, *Nat. Chem.*, 2017, **9**, 689–697.
33 C. P. Joshi, M. S. Bootharaju and O. M. Bakr, *J. Phys. Chem. Lett.*, 2015, **6**, 3023–3035.
34 M. Ganguly, C. Bradsher, P. Goodwin and J. T. Petty, *J. Phys. Chem. C*, 2015, **119**, 27829–27837.
35 J. T. Petty, M. Ganguly, I. J. Rankine, D. M. Chevrier and P. Zhang, *J. Phys. Chem. C*, 2017, **121**, 14936–14945.
36 L. G. AbdulHalim, N. Kothalawala, L. Sinatra, A. Dass and O. M. Bakr, *J. Am. Chem. Soc.*, 2014, **136**, 15865–15868.
37 S. Jin, S. Wang, Y. Song, M. Zhou, J. Zhong, J. Zhang, A. Xia, Y. Pei, M. Chen, P. Li and M. Zhu, *J. Am. Chem. Soc.*, 2014, **136**, 15559–15565.
38 S. Choi and J. Yu, *APL Mater.*, 2017, **5**, 053401.
39 R. X. Jin, S. Zhao, Y. Xing and R. C. Jin, *CrystEngComm*, 2016, **18**, 3996–4005.
40 W. Matz, N. Schell, G. Bernhard, F. Prokert, T. Reich, J. Claussner, W. Oehme, R. Schlenk, S. Dienel, H. Funke, F. Eichhorn, M. Betzl, D. Prohl, U. Strauch, G. Huttig, H. Krug, W. Neumann, V. Brendler, P. Reichel, M. A. Denecke and H. Nitsche, *J. Synchrotron Radiat.*, 1999, **6**, 1076–1085.
41 M. Borsboom, W. Bras, I. Cerjak, D. Detollenaere, D. Glastra Van Loon, P. Goedtkindt, M. Konijnenburg, P. Lassing, Y. K. Levine, B. Munneke, M. Oversluizen, R. Van Tol and E. Vlieg, *J. Synchrotron Radiat.*, 1998, **5**, 518–520.
42 E. Coutino-Gonzalez, D. Grandjean, M. Roeffaers, K. Kvashnina, E. Fron, B. Dieu, G. De Cremer, P. Lievens, B. Sels and J. Hofkens, *ChemComm*, 2014, **50**, 1350–1352.
43 N. Binsted, J. Campbell, S. J. Gurman and P. C. Stephenson, *EXAFS analysis Programs*, Daresbury Laboratory, Warrington, U.K., 1991.
44 K. Beck, H. Pfeifer and B. Staudte, *Microporous Mater.*, 1993, **2**, 1–6.
45 Y. Wang and N. Herron, *J. Phys. Chem.*, 1988, **92**, 4988–4994.
46 H. Lin, K. Imakita, M. Fujii, V. Y. Prokof'ev, N. E. Gordina, B. Said and A. Galarneau, *Nanoscale*, 2015, **7**, 15665–15671.
47 H. Lin, K. Imakita, S. C. Rong Gui and M. Fujii, *J. Appl. Phys.*, 2014, **116**, 013509.
48 H. Lin, K. Imakita and M. Fujii, *Appl. Phys. Lett.*, 2014, **105**, 211903.
49 G. Calzaferri, C. Leiggener, S. Glaus, D. Schurch and K. Kuge, *Chem. Soc. Rev.*, 2003, **32**, 29–37.
50 R. Seifert, R. Rytz and G. Calzaferri, *J. Phys. Chem. A*, 2000, **104**, 7473–7483.
51 R. Seifert, A. Kunzmann and G. Calzaferri, *Angew. Chem., Int. Ed.*, 1998, **37**, 1522–1524.
52 J. Michalik and L. Kevan, *J. Am. Chem. Soc.*, 1986, **108**, 4247–4253.
53 G. E. Pavlovskaya, C. F. Horton-Garcia, C. Dybowski, D. R. Corbin and T. Meersmann, *J. Phys. Chem. B*, 2004, **108**, 1584–1589.
54 J. C. Fierro-Gonzalez, S. Kuba, Y. Hao and B. C. Gates, *J. Phys. Chem. B*, 2006, **110**, 13326–13351.
55 V. Bolis, A. Barbaglia, S. Bordiga, C. Lamberti and A. Zecchina, *J. Phys. Chem. B*, 2004, **108**, 9970–9983.
56 T. Miyamoto, H. Niimi, Y. Kitajima, T. Naito and K. Asakura, *J. Phys. Chem. A*, 2010, **114**, 4093–4098.
57 P. Behrens, S. Aßmann, U. Bilow, C. Linke and M. Jansen, *Z. Anorg. Allg. Chem.*, 1999, **625**, 111–116.
58 E. Coutino-Gonzalez, W. Baekelant, J. A. Steele, C. W. Kim, M. B. J. Roeffaers and J. Hofkens, *Acc. Chem. Res.*, 2017, **50**, 2353–2361.
59 B. B. Iversen, S. Latturner and G. Stucky, *Chem. Mater.*, 1999, **11**, 2912–2918.
60 J. E. Sponer, Z. Sobalik, J. Leszczynski and B. Wichterlova, *J. Phys. Chem. B*, 2001, **105**, 8285–8290.
61 S. E. Latturner, J. Sachleben, B. B. Iversen, J. Hanson and G. D. Stucky, *J. Phys. Chem. B*, 1999, **103**, 7135–7144.
62 J. H. Kwaka, T. Vargab, C. H. F. Pedenc, F. Gaoc, J. C. Hansond and J. Szany, *J. Catal.*, 2014, **314**, 83–93.
63 R. A. Schoonheydt and H. Leeman, *J. Phys. Chem.*, 1989, **93**, 2048–2053.
64 D. Grandjean, E. Coutino-Gonzalez, N. T. Cuong, E. Fron, W. Baekelant, M. S. Aghakhani, P. Schlexer, F. D'Acapito, D. Banerjee, M. B. J. Roeffaers, M. T. Nguyen, J. Hofkens and P. Lievens, *Science*, 2017, in revision.
65 L. R. Gellens, W. J. Mortier, R. Lissillour and A. Le Beuze, *J. Phys. Chem.*, 1982, **86**, 2509–2516.

66 G. Zhang, X. Liu and J. K. Thomas, *Radiat. Phys. Chem.*, 1997, **51**, 135–152.
67 M. Álvaro, J. F. Cabeza, D. Fabuel, H. García, E. Guijarro and J. L. Martínez de Juan, *Chem. Mater.*, 2006, **18**, 26–33.
68 N. Cvjeticanin, S. Mentus and N. Petranovic, *Solid State Ionics*, 1991, **47**, 111–115.
69 P. A. Jacobs and J. B. Uytterhoeven, *J. Chem. Soc., Faraday Trans. 1*, 1979, **75**, 56–64.
70 P. Wang, S. Yang, J. N. Kondo, K. Domen and T. Baba, *Bull. Chem. Soc. Jpn.*, 2004, **77**, 1627–1634.
71 N. Atsushi, N. Masataka, N. Sho, S. Yushi and M. Takafumi, *J. Phys.: Conf. Ser.*, 2014, **502**, 012033.
72 L. Gell, L. Lehtovaara and H. Hakkinen, *J. Phys. Chem. A*, 2014, **118**, 8351–8355.
73 M. V. Shestakov, N. T. Cuong, V. K. Tikhomirov, M. T. Nguyen, L. F. Chibotaru and V. V. Moshchalkov, *J. Phys. Chem. C*, 2013, **117**, 7796–7800.
74 A. Kulesza, R. Mitric, V. Bonacic-Koutecky, B. Bellina, I. Compagnon, M. Broyer, R. Antoine and P. Dugourd, *Angew. Chem., Int. Ed.*, 2011, **50**, 878–881.
75 H. C. Yeh, J. Sharma, J. J. Han, J. S. Martinez and J. H. Werner, *Nano Lett.*, 2010, **10**, 3106–3110.
76 Y. Yu, B. Y. Mok, X. J. Loh and Y. N. Tan, *Adv. Healthcare Mater.*, 2016, **5**, 1844–1859.